Radiative Effects of African Dust and Smoke Observed from CERES and CALIOP Data

John E. Yorks[1], Matt McGill[2], Sharon Rodier[3], Mark Vaughan[4], Yongxiang Hu[4], Dennis Hlavka[1]

[1]Science Systems and Applications, Inc. at NASA Goddard Space Flight Center
[2]NASA Goddard Space Flight Center
[3]Science Systems and Applications, Inc. at NASA Langley Research Center
[4]NASA Langley Research Center

ABSTRACT: Cloud and aerosol effects have a significant impact on the atmospheric radiation budget in the Tropical Atlantic because of the spatial and temporal extent of desert dust and smoke from biomass burning in the atmosphere. The influences of African dust and smoke aerosols on cloud radiative properties over the Tropical Atlantic Ocean were analyzed for the month of July for three years (2006-2008) using collocated data collected by the Cloud-Aerosol Lidar with Orthogonal Polarization (CALIOP) and Clouds and the Earth's Radiant Energy System (CERES) instruments on the CALIPSO and Aqua satellites. Aerosol layer height and type can be more accurately determined using CALIOP data, through parameters such as cloud and aerosol layer height, optical depth and depolarization ratio, than data from atmospheric imagers used in previous cloud-aerosol interaction studies. On average, clouds below 5 km had a daytime instantaneous shortwave (SW) radiative flux of 270.2 ± 16.9 W/m^2 and thin cirrus clouds had a SW radiative flux of 208.0 ± 12.7 W/m^2. When dust aerosols interacted with clouds below 5 km, as determined from CALIPSO, the SW radiative flux decreased to 205.4 ± 13.0 W/m^2. Similarly, smoke aerosols decreased the SW radiative flux of low clouds to a value of 240.0 ± 16.6 W/m^2. These decreases in SW radiative flux were likely attributed to the aerosol layer height and changes in cloud microphysics. CALIOP lidar observations, which more accurately identify aerosol layer height than passive

instruments, appear essential for better understanding of cloud-aerosol interactions, a major uncertainty in predicting the climate system.

1. Introduction

Clouds and aerosols can have numerous effects on the atmospheric radiation budget. Clouds, especially at large optical depths, can potentially cause large negative net radiative forcing (cooling) because the radiation backscattered to space often exceeds the cloud greenhouse effect (Rajeevan et al., 1999). During cloud-free conditions, aerosols such as desert dust and smoke from biomass burning reflect solar radiation to space and absorb radiation, processes known as the aerosol direct radiative effect (Haywood et al., 2000). The uncertainty in understanding cloud and aerosol effects on the radiation budget results from complex interactions between aerosols and clouds. High concentrations of dust and smoke particles act as ice nuclei (IN) in cirrus clouds and cloud condensation nuclei (CCN) in water clouds (Kaufman et al., 1997; DeMott et al., 2003). Consequently, clouds that form in the presence of high aerosol concentrations tend to contain more numerous but smaller droplets that can increase cloud albedo and suppress precipitation (Ackerman et al., 2000; Rosenfeld et al., 2001). These phenomena are defined as the aerosol indirect radiative effect (Twomey, 1977; Albrecht, 1989). The aerosol semi-direct effect arises when aerosols heat the atmosphere, evaporating low-level clouds (Grassl, 1975; Su et al., 2008). Also, dust and smoke layers elevated above low-level clouds can inhibit solar radiation from reaching a cloud layer through aerosol absorption. These cloud and aerosol effects on

the atmospheric radiation budget remain a major uncertainty in understanding and predicting the climate system (Solomon et al., 2007).

The interactions between aerosols and clouds can have an important effect on the Earth's radiation balance in regions such as the Tropical Atlantic due to the large spatial and temporal extent of desert dust and smoke in the atmosphere. Biomass burning in the tropics is responsible for roughly 80% of the globally burned biomass, making Africa a major source of carbon containing smoke aerosols in the global atmosphere (Keil et al., 2003). During August-September 2000, the Southern Africa Regional Science Initiative (SAFARI; Swap et al., 2002) was conducted to further investigate the smoke aerosols generated from biomass burning in this region. During the dry season (June-September) over land, anticyclonic systems cause stagnant conditions and extend aerosol residence time (Ross et al., 2003). Along coastal regions, trade winds transport smoke aerosols over the Atlantic Ocean between the Equator and 20 S (Myhre et al., 2003). Africa also contains the Earth's largest desert, the Sahara, a significant source for atmospheric desert dust. Saharan dust greatly influences the Northern Tropical Atlantic (5 N-30 N) in July (Kaufman et al., 2005) and long-range transport of dust from Africa can even contribute to high fine aerosol mass concentrations in the U.S. during the summer months (DeMott et al., 2003). The NASA African Monsoon Multidisciplinary Analyses (NAMMA; Redelsperger et al., 2006) field campaign was performed in August of 2006 to examine the effect of this dust on tropical precipitation and tropical cyclone development. Although the cloud microphysical and radiative effects of these African aerosols have been studied during projects such as

SAFARI and NAMMA, there are few investigations of these radiative effects over the Tropical Atlantic as seen from recent satellite observational lidar data.

In recent years, several studies have investigated the radiative effects of clouds and Asian dust. Huang et al. (2006a) used Clouds and the Earth's Radiant Energy System (CERES) and the Moderate Resolution Imaging Spectroradiometer (MODIS) data to examine the impacts of Asian dust storms on radiative forcing and cloud microphysics in cloudy conditions. Su et al. (2008) conducted a similar study by using additional Asian dust storm cases and the Fu-Liou radiative model. Both studies found that, on average, SW and net instantaneous top-of-atmosphere (TOA) radiative forcing in regions with dust and clouds present were less negative than aerosol-free cloudy regions. It is also revealed from these studies that changes in cloud microphysical properties, such as decreases in optical depth, corresponded to changes in SW and net radiative forcing. However, identifying dust-contaminated ice clouds is a challenge for MODIS cloud mask algorithms (Brennan et al., 2005). The identification of dust-contaminated clouds in these studies assumes the cloud is dust-contaminated when the brightness temperature for ice clouds at the 11 μm becomes larger than the brightness temperature at 12 μm (Huang et al., 2006a). However, if water clouds are located beneath the ice cloud layer, a situation commonly observed in the tropics, this assumption is invalid. In this study, we will examine data from the CERES instrument and Cloud-Aerosol Lidar with Orthogonal Polarization (CALIOP) instrument on the Cloud-Aerosol Lidar Infrared Pathfinder Satellite Observations (CALIPSO) satellite to quantify the impacts of African dust and smoke on radiative properties of clouds, resolve the prominent aerosol radiative effects in the Tropical Atlantic, and demonstrate the

ability of the CALIOP data to more accurately determine the aerosol layer height and type. Ultimately, this lidar data should lead to a better understanding of aerosol-cloud-climate interactions over the Tropical Atlantic.

2. Data and Methodology

The launch of the CALIPSO satellite in April 2006 allows the science community to explore aerosol-cloud interactions through parameters such as cloud and aerosol layer height, optical depth and depolarization ratio. The primary instrument on the CALIPSO satellite is the dual wavelength, polarization-sensitive backscatter lidar known as CALIOP. This lidar measures vertical profiles of cloud and aerosol optical properties in the atmosphere with a vertical resolution of 60 meters in the troposphere (Winker et al., 2009). The level 2 cloud and aerosol data with 5 km horizontal resolution is analyzed in this study. Parameters of interest such as cloud and aerosol height, integrated attenuated backscatter, optical depth, and depolarization ratio are obtained from the backscatter data. The CALIPSO satellite provides global vertical profile measurements of clouds and aerosols to complement the horizontal plane data acquired by existing imagers on NASA satellites. CALIPSO orbits in formation with the Aqua satellite as part of the NASA A-Train satellite constellation, a group of six satellites that fly in close proximity. This allows examination of Earth's climate system by combining the CALIPSO data set with other platforms such as CERES (Hu et al., 2007; Hu et al., 2008; Eckhardt et al., 2008).

CERES, a payload on the Aqua satellite, supplies the science community with global radiance measurements. The instrument measures broadband TOA radiances at a spatial resolution of 20 km at nadir in three spectral regions; 0.2 to 5 μm, 8 to 12 μm,

0.2 to 100 μm. The first of the three bands measures shortwave (SW) broadband radiation, while the third band measures total broadband radiation. Longwave (LW) broadband radiation is then estimated as the total minus the shortwave (Wielicki et al., 1996). These SW and LW radiances are then converted to atmospheric and surface fluxes using angular distribution models, which correct for bi-directional properties of a reflecting surface (Loeb et al., 2005). CERES provides the most accurate set of global radiative fluxes at TOA and the surface to date. CERES Single Scanner Footprint (SSF) data sets combine CERES radiation measurements and MODIS cloud microphysical retrievals to create a set of 140 parameters for studying the role of clouds in the Earth's radiation budget (Huang et al., 2006a).

We have collocated the CALIOP 5 km laser footprint and the CERES SSF 20 km nadir pixel for the month of July for three years, 2006 through 2008. The geographical area the data represents is 22 S to 28 N latitude and 35 W to 10 W longitude, over the Atlantic ocean. This data fusion was possible because the CALIPSO and Aqua satellites were so close in proximity that a point on the ground will be observed by the CALIOP and CERES instruments with an average time separation of 1.5 minutes (Winker et al., 2003). The collocation was achieved via a two-step process (Holz et al., 2008). Data was first collocated in time, and then in space. The CALIOP position information was used to find the best matching CERES footprint within 0.25 degrees from its footprint. Once a match was found, a location offset from the CALIOP footprint was calculated and stored. All selected SSF parameters were merged with the CALIOP 5 km data product for further analysis.

The CERES-CALIOP collocated data set offered many advantages compared to the measurements provided by the CERES-MODIS SSF data. First, CALIOP provides vertical profiles with vertical resolution of 60 meters to correctly detect multiple cloud and aerosol layers in a single profile. This task is important when studying cloud-aerosol interaction but can be difficult using an imager such as MODIS. Once these cloud and aerosol layers were detected, it was essential to identify the type of cloud or aerosol, since radiative effects are largely governed by the cloud and aerosol physical and optical properties. The cloud and aerosol type is more accurately determined using CALIOP than MODIS through parameters such as layer height, depolarization ratio, color ratio, and extinction-to-backscatter ratio (S-ratio). However, combining two data sets with varying horizontal and vertical resolution can introduce some uncertainties. Therefore, horizontal homogeneity must be assumed across the 20 km CERES footprint to make direct comparisons between instruments. To this end, only profiles with a cloud layer detected by CALIOP and a CERES subpixel percent area overcast value between 85% and 100% were considered cloudy profiles. Also, only profiles with an aerosol layer measured by CALIOP and a CERES subpixel percent area overcast value greater than 25% were considered aerosol polluted profiles. For opaque clouds that completely attenuate the signal, CALIOP, like most lidar systems, does not have the signal strength to measure the full extent of the cloud. Consequently, this study only examined transparent clouds. In order to correctly obtain the optical depths of transparent clouds and aerosols from the CALIOP lidar, estimations of the multiple scattering and extinction-to-backscatter ratio must be accurate (Zardecki et al., 1983). However, the multiple scattering factor used to obtain the optical depth of water clouds in the

CALIPSO version 2.01 data product is incorrect, leading to unreliable retrievals of cloud optical depth for water clouds (Winker et al., 2009). CALIOP extinction profiles (i.e. optical depth) for ice clouds, as well as cloud integrated attenuated backscatter, layer top and base altitude for all clouds are found to be consistent with those determined by the airborne Cloud Physics Lidar (McGill et al., 2007; Hlavka et al., 2009) and therefore will be included in this analysis.

The local daytime CALIPSO track (typically around 1400 to 1600 UTC) of the collocated data was analyzed and separated into ten profile types. These profile types, explained in Table 1, were computed based on the optically thickest cloud and aerosol layers detected in the profile and were determined separately from the CALIPSO feature mask product. The 532 nm total attenuated backscatter (km^{-1}/sr^{-1}) from CALIOP for 17 July, 2007 appears in Figure 1, with black boxes to demonstrate the cloud and aerosol layers used to define the ten profile types. A thin cirrus cloud was defined as a cloud with optical depth between 0.1 and 1.0 and a base height higher than 8 km. It should be noted that cirrus clouds can have optical depths above 1.0, however, aerosol layers located underneath these thicker cirrus were difficult to detect. All other clouds above 5 km with an optical depth greater than 1.0 were considered high convective clouds (HCC). Table 1 shows only one profile type based on high convective clouds because aerosols were rarely observed in the same profile since these clouds attenuate a large portion of the lidar signal. Clouds below 5 km were designated “Low Cloud”. Dust, typically lofted in this analysis as shown in Figure 1, was classified as an aerosol layer with a depolarization ratio greater than 0.20, or between 0.07 and 0.20 with an S-ratio between 40 and 60. When the depolarization ratio was less than 0.07 or between

0.07 and 0.20 with an S-ratio greater than 60, these layers were assigned as “Smoke”. When no cloud or aerosol layers are detected by CALIOP, the profile is considered “Clear”. The aforementioned profile types will be used to determine the direct radiative effects of these clouds and aerosols. The remaining four profile types (Table 1) will consist of profiles in which both a cloud and aerosol layer were detected, providing a basis for studying the semi-direct effect of smoke and dust aerosols.

3. Results

3.1 Cloud Observations and Aerosol Transport

Dust and smoke from Africa were prominent over the Tropical Atlantic during July (2006 to 2008), creating the opportunity for cloud-aerosol interactions. To assess the distribution of the cloud and aerosol layer locations and confirm the layers used in this study were consistent with previous studies, the frequencies of the latitudinal occurrence of these layers were plotted in Figure 2. This figure stresses the most frequent latitudes in which a layer type occurs relative to all latitudes in which that layer type was observed for this study. Low clouds, mostly marine boundary layer cumulus clouds, were detected throughout the Tropical Atlantic on all days analyzed (Figure 2). High convective and thin cirrus clouds (“High Clouds”) were primarily observed in the region of the ITCZ, centered at about 7 N (Figure 2). Clouds in these locations were also observed in Figure 1, with a thin cirrus cloud north of the ITCZ. The Northern Tropical Atlantic (28 N to 10 N) was heavily influenced by dust (Figure 2). For example, on 17 July 2007, an elevated, optically-thick dust layer was observed off the northwestern coast of Africa between 27 N and 17 N (Figure 1). Back trajectories initialized at 18 N, 25 W for 17 July 2007 at 1500 UTC revealed 4.0 km (green) and 2.0

km (yellow) flow from the low-level Sahara Desert region, further verifying the lofted layer was dust from Saharan sources (Figure 3). Back trajectories for everyday in July (2006-2008) also suggested the Saharan boundary layer as the source of the dust layers observed in Figure 2, which compared favorably with the results of Kaufman et al. (2005) and Engelstaedter et al. (2007). In addition, aerosol layers, likely a mixture of sea salt and smoke aerosols, were prevalent during July in the marine boundary layer from 4 N to 22 S (Figure 2), similar to the findings of Myhre et al. (2003). The source of these smoke layers in Figure 1 and 2 were likely attributed to biomass burning in southern Africa, as back trajectories from everyday in July (2006-2008) indicated influence from southern Africa. For example, on 17 July 2007, back trajectories initialized at 2 S, 20 W demonstrated low-level (0.5 km, red; 1.0 km, blue) flow from southern Africa where MODIS detected a large amount of active fires on this day (Figure 3). Carbon Monoxide (CO) increases during the month of July compared to previous months in southern Africa have been modeled and observed due to savanna burning in Sahel (Bremer et al., 2004). The locations of cloud and aerosol layers determined in this study were consistent with previous results and can be used to evaluate differences in radiative fluxes.

3.2 Cloud and Aerosol Direct Radiative Effects

In the absence of clouds, aerosols such as smoke and dust scattered solar radiation back to space, causing a cooling effect compared to clear, pristine conditions. Figure 4 shows the 2006, 2007, 2008 and 3-year mean instantaneous TOA SW radiative fluxes for all cloud-free profiles. Over the Tropical Atlantic, clear and pristine skies had a 3-year mean SW radiative flux of 74.0 ± 1.1 W/m^2. Cloud-free profiles

containing smoke and dust layers yielded a 3-year mean of 141.5 ± 7.4 and 161.9 ± 23.4 W/m^2, respectively, increases of 90% and 118% compared to clear and pristine conditions. To within the uncertainties inherent in the retrievals, the mean optical depths of dust and smoke layers were nearly equivalent (Table 2), but the higher SW radiative flux of dust (13% higher than smoke) indicates it backscattered more SW radiation than smoke, likely due to less absorption compared to the absorption properties of black carbon particles in smoke layers. Supporting this notion, Cess (1985) reported a single scattering albedo at 550 nm of 0.70 for smoke, lower than the 0.98 value of dust. In the longwave, the smoke aerosols (280.7 ± 6.1 W/m^2) caused a decrease in TOA radiative flux compared to clear skies (294.7 ± 0.9 W/m^2), but only by about 5%. Therefore, when aerosols were observed in the Tropical Atlantic, the scattering of solar radiation back to space was more dominant than the greenhouse effect.

The presence of clouds in the atmosphere had a large impact on radiative effects. To compare the impact on radiative effects for different profile types, the 2006, 2007, 2008 and 3-year mean instantaneous TOA SW and LW radiative fluxes for all cloud profiles is displayed in Figures 5a and 5b, respectively. Profiles in which high convective clouds were detected had the most substantial impact on radiative forcing. These profiles yielded a 3-year mean SW radiative flux of 359.7± 19.3 W/m^2, about 285 W/m^2 greater than clear, pristine skies, whereas the 3-year mean LW radiative flux was nearly 90 W/m^2 less than clear, pristine profiles. The 3-year mean SW radiative flux for low cloud and thin cirrus cloud profiles were 271.5 ± 16.9 and 208.0 ± 12.7 W/m^2, respectively. The low cloud profiles had a greater cooling effect than the optically thin

cirrus clouds observed in this study, likely a characteristic of the larger integrated attenuated backscatter observed in low clouds. Table 3 shows a 3-year mean integrated attenuated backscatter of 0.0570 ± 0.0032 sr^{-1} for low clouds, but only 0.0152 ± 0.0002 sr^{-1} for the thin cirrus profiles. Rajeevan et al. (1999) demonstrated that clouds with large optical depths have a large negative (cooling) net cloud forcing because the effect of cloud albedo exceeds the cloud greenhouse effect. However, thin cirrus clouds had a stronger greenhouse effect than low clouds. The 3-year mean LW radiative flux for thin cirrus clouds was 217.8 ± 7.5 W/m^2, which was 15% lower than Low Cloud profiles and 26% lower than clear, pristine profiles (Figure 5b). This was likely attributed to the difference in cloud height between thin cirrus (11.75 ± 0.38 km) and low clouds (1.93 ± 0.50 km) in Table 3, an association that was shown by Weare (1997). The stronger greenhouse effect of these thin cirrus indicates a weaker net cooling effect compared to low clouds, which ultimately demonstrates the importance of low clouds on the climate system. When these low clouds were formed in air laden with aerosols, the radiative effects became more complex.

3.3 Cloud and Aerosol Interactions

The presence of aerosols in profiles with low clouds or thin cirrus clouds weakened the SW cooling effect of these clouds. However, these radiative effects could have originated from different mechanisms due to the aerosol characteristics of dust and smoke layers over the Tropical Atlantic. Table 3 reports mean cloud properties for all six cloud profile types. All variables in Table 3 are obtained by the CALIOP lidar except cloud optical depth for low cloud profiles, which are not available (NA) for reasons explained in section 2.

Profiles in which both dust and low clouds were observed yielded a 3-year mean SW radiative flux of 205.4 ± 13.0 W/m^2, about 25% less than aerosol-free low cloud profiles (Figure 5a). The normalized frequency of the altitude of the dust and cloud layers from DLC profiles (Figure 6a) suggests the height of the dust layer played a significant role in the aerosol-cloud interaction. In DLC profiles, over 80% of cloud layers were observed below 2.0 km. Whereas, approximately 86% of dust layers were found above 2.0 km and above the majority of cloud layers. These dust layers absorbed and scattered solar radiation, which likely decreased the amount of solar radiation that reached the cloud, warmed the air in the vicinity of cloud top, and evaporated cloud particles located in the upper part of the cloud (the semi-direct effect). Huang et al. (2006b) showed that changes in cloud microphysics reduce the cloud cooling effect, dominated by the aerosol semi-direct effect. This appears evident, since the mean cloud integrated attenuated backscatter (CIAB, 0.0324 ± 0.0015 sr^{-1}) of DLC profiles was about 43% less than Low Cloud profiles (Table 3). To put these values in another prospective, with inherent uncertainty, if we assume an extinction of 1.0 for water clouds and an identical multiple scattering factor for both cases, a rough estimate of extinction-to-backscatter ratio would be 17.5 for low clouds and 30.9 for dust contaminated low clouds. A running average of low cloud SW radiative flux is plotted as a function of aerosol layer height for DLC and SLC profiles in Figure 7a and 7b. Dust layers between 1.5 and 2.0 km, just above the majority of cloud layers, yield SW radiative fluxes below 200 W/m^2 and the SW radiative flux is below 225 W/m^2 for dust layers of all heights. Ultimately, the weakening of net low cloud cooling observed was dictated by two factors; absorption and multidirectional scattering by dust layers a few

kilometers above low clouds and changes in cloud microphysics initiated by the semi-direct effect of dust layers in close proximity to low clouds. The influence of aerosols on LW radiative effects of low clouds, already weak forcing compared to thin cirrus clouds, was minimal because aerosols only increased LW radiative flux by less than 5% (Figure 5b).

Similar to dust layers, the SW radiative flux of low clouds decreased in the presence of smoke layers while the LW flux was relatively insensitive to the presence of smoke layers in low cloud profiles (Figure 5b). The 3-year mean SW radiative flux for SLC profiles was 240.0 ± 16.6 W/m^2, nearly 30 W/m^2 less than Low Cloud profiles (Figure 5a). About half (55%) of smoke layers were found below 2.0 km, at the same level as the majority (82%) of the cloud layers, as illustrated in Figure 6b, the normalized frequency of the altitude of the smoke and cloud layers from SLC profiles. The mean cloud integrated attenuated backscatter (0.0374 ± 0.0087 sr^{-1}) for SLC profiles was nearly 35% lower than Low Cloud profiles (Table 3) and the inferred extinction-to-backscatter ratio (26.7) was higher than Low Cloud profiles. Figure 7b shows significantly lower mean SW radiative flux for profiles with smoke layers below 2 km than profiles with smoke layers at any other height. Also, the running average of SW radiative flux was greater than 225 W/m^2 for smoke layers above 2 km, yet never reach the 271.5 ± 16.9 W/m^2 value for aerosol-free low clouds. Therefore, it appears that smoke layers are likely interacting with low clouds off the West African coast, causing a decrease in low cloud cooling, the semi-direct effect. However, these radiative effects are most prevalent for smoke layers below 2.0 km, unlike the dust radiative effects which are observed resulting from dust layers of all heights. Analyzing

the aerosol layer height with respect to the cloud height (Figures 6 and 7) was critical in deriving the complex cloud-aerosol interactions that induced changes in radiative effects. This analysis cannot be done using a passive A-Train instrument, illustrating the importance of the CALIOP lidar in a study of this nature.

It is possible that radiative effects of thin cirrus clouds could have been influenced by dust and smoke layers, despite the fact that thin cirrus clouds were typically 5 to 9 km higher than these aerosol layers. The 3-year mean SW radiative fluxes for DC and SC profiles were 183.8 ± 16.2 W/m^2 and 167.7± 19.4 W/m^2, respectively (Figure 5). These values were 12% and 20% less than the 208.0 ± 12.7 W/m^2 of thin cirrus profiles (Figure 5). The greenhouse effect of thin cirrus clouds was also significant. SC and DC profiles have mean LW radiative fluxes of about 235 W/m^2, nearly 7% greater than the value of 217.8 ± 7.5 W/m^2 for aerosol-free thin cirrus cloud profiles (Figure 6). It should be mentioned that the mean thin cirrus height for aerosol-free profiles is about 0.5 km lower than aerosol-cirrus profiles, which could have caused the difference in mean LW radiative flux between these profiles. Su et al. (2008) suggested that reduced cooling due to the existence of dust under clouds can be considered as a warming effect of these aerosols through dust absorption. Since the mean cloud optical depths and cloud integrated attenuated backscatter for SC and DC profiles were over 25% less than thin cirrus profiles, it is possible that changes in cloud microphysics also contributed to changes in SW radiative flux observed (Table 3). Although the impact of the semi-direct effect of smoke and dust layers on cirrus clouds can be observed from CALIPSO cloud properties, it is difficult to confirm that these effects are solely a result of the presence of aerosol layers and not an artifact of the

small sample sizes of the DC and SC bins or the meteorological conditions in which the dust and smoke layers were transported. However, Su et al. (2008) used the Fu-Liou radiation model, during a study of dust semi-direct radiative effect on cirrus clouds, to demonstrate that 78.4% of the total aerosol radiative forcing can be attributed to aerosol indirect and semi-direct effects. Also, Twohy et al. (2009) showed Saharan dust acts as cloud condensation and ice nuclei in clouds off the west coast of Africa through observations taken during the NAMMA field campaign.

4. Conclusion

Dust and smoke from African sources are transported into the Tropical Atlantic atmosphere, where they interact with marine boundary layer and thin cirrus clouds. These cloud-aerosol interactions influence the atmospheric radiation budget and climate system. Phenomena such as aerosol indirect and semi-direct effects can occur, but few studies have demonstrated these effects as seen from observational data. Therefore, cloud-aerosol interaction remains a major uncertainty in understanding the climate system. The launch of the CALIPSO satellite has made it possible to detect aerosol and cloud layers in high-resolution vertical profiles using the CALIOP backscatter lidar.

Individual aerosol and cloud layers over the Tropical Atlantic resulted in stronger SW radiative cooling, and stronger greenhouse effects compared to clear and pristine conditions. These radiative effects were altered when African dust and smoke layers interacted with marine boundary layer and thin cirrus clouds over the Tropical Atlantic. When dust or smoke layers existed below thin cirrus clouds, the SW radiative flux decreased by about 12-20% compared to aerosol-free thin cirrus clouds. This is likely due to aerosol absorption below the cloud, but changes in cloud microphysics may have

played a role in aerosol-cirrus cloud interactions as well. The more profound impact is found at the lower levels. Profiles with dust and low clouds present had a 3-year mean SW radiative flux of 205.4 ± 13.0 W/m^2, about 25% less than aerosol-free low cloud profiles. This appears to be a result of dust layers elevated above low clouds which absorb solar radiation, inhibit radiation from reaching the cloud and evaporate cloud particles within the cloud. This decrease in low cloud SW radiative flux due to elevated Saharan dust layers induced a weakening of low cloud cooling in excess of 30%, exhibiting the importance in understanding the influence of cloud-aerosol interactions on the radiation budget and climate system. Similarly, the SW radiative flux for SLC profiles was 12% less than Low Cloud profiles. However, changes in cloud microphysics were likely the dominant effect since mean cloud integrated attenuated backscatter for SLC profiles were nearly 25% lower than aerosol-free low cloud profiles. The aerosol layer height and type are critical factors in determining cloud-aerosol interactions and are better detected using the CALIOP lidar data than any other A-Train instrument.

Acknowledgments. NASA's Radiation Sciences Program funded this study. Special thanks to all the members of the CALIPSO and CERES science team for making the instrument data available.

References

Ackerman, A. S., et al. (2000), Reduction of tropical cloudiness by soot, Science, 288, 1042–1047.

Albrecht, B. A. (1989), Aerosols, cloud microphysics, and fractional cloudiness, Science, 245, 1227–1230.

Bremer, H., Kar, J., Drummond, J. R., Nichitu, F., Zou, J., Liu, J., J. C. Gille, J. C., Deeter, M. N., Francis, G., Ziskin, D., and J. Warner (2004), The Spatial and Temporal Variation of MOPITT CO in Africa and South America: A Comparison With SHADOZ Ozone and MODIS Aerosol, J. Geophys. Res., 109(D12), D12304, doi:10.1029/2003JD004234.

Brennan, J.I., Y.J. Kaufman, I. Koren, and R.-R. Li (2005), Aerosol-cloud interaction — misclassification

of MODIS clouds in heavy aerosol, IEEE Transactions on Geoscience and Remote Sensing, 43, 911-915.

Cess, R. D. (1985), Nuclear war: illustrative effects of atmospheric smoke and dust upon solar radiation, Climatic Change 7 (1985), 237–251.

DeMott, P. J., K. Sassen, M. R. Poellot, D. Baumgardner, D. C. Rogers, S. D. Brooks, A. J. Prenni, and S. M. Kreidenweis (2003), African dust aerosols as atmospheric ice nuclei, Geophys. Res. Lett., 30(14), 1732, doi:10.1029/2003GL017410.

Eckhardt, S., A. J. Prata, P. Seibert, K. Stebel, and A. Stohl (2008), Estimation of the vertical profile of sulfur dioxide injection into the atmosphere by a volcanic eruption using satellite column measurements and inverse transport modeling, Atmos. Chem. Phys., 8, 3881–3897.

Engelstaedter, S., and R. Washington (2007), Atmospheric controls on the annual cycle of North African dust, J. Geophys. Res., VOL. 112, D03103, doi:10.1029/2006JD007195.

Grassl, H. (1975), Albedo Reduction and Radiative Heating of Clouds by Absorbing Aerosol Particles, Contrib. Atmos. Phys., 48, 199–210.

Haywood, J. M., and O. Boucher (2000), Estimates of the direct and indirect radiative forcing due to tropospheric aerosols: A review, Rev. Geophys., 38, 513–543.

Holz, R. E., S. A. Ackerman, F. W. Nagle, R. Frey, S. Dutcher, R. E. Kuehn, M. A. Vaughan, and B. Baum (2008), Global Moderate Resolution Imaging Spectroradiometer (MODIS) cloud detection and height evaluation using CALIOP, J. Geophys. Res., 113, D00A19, doi:10.1029/2008JD009837.

Hlavka, D.L. et al. (2009), Validation of CALIPSO level 2 data products using the Cloud Physics Lidar, in preparation.

Hu, Y., M. Vaughan, C. McClain, M. Behrenfeld, H. Maring, D. Anderson, S. Sun-Mack, D. Flittner, J. Huang, B. Wielicki, P. Minnis, C. Weimer, C. Trepte, and R. Kuehn (2007), Global statistics of liquid water content and effective number concentration of water clouds over ocean derived from combined CALIPSO and MODIS measurements, Atmos. Chem. Phys., 7, 3353–3359.

Hu, Y., K. Stamnes, M. Vaughan, J. Pelon, C. Weimer, D. Wu, M. Cisewski, W. Sun, P. Yang, B. Lin, A. Omar, D. Flittner, C. Hostetler, C. Trepte, D. Winker, G. Gibson, and M. Santa-Maria (2008), Sea surface wind speed estimation from space-based lidar measurements, Atmos. Chem. Phys., 8, 3593–3601.

Huang, J., P. Minnis, B. Lin, T. Wang, Y. Yi, Y. Hu, S. Sun-Mack, and K. Ayers (2006a), Possible influences of Asian dust aerosols on cloud properties and radiative forcing observed from MODIS and CERES, Geophys. Res. Lett., 33, L06824, doi:10.1029/2005GL024724.

Huang, J., B. Lin, P. Minnis, T. Wang, X. Wang, Y. Hu, Y. Yi, and J. K. Ayers (2006b), Satellite-based assessment of possible dust aerosols semi-direct effect on cloud water path over East Asia, Geophys. Res. Lett., 33, L19802, doi:10.1029/2006GL026561.

Kaufman Y.J., D. Tanré, L. A. Remer, E. Vermote, A. Chu and B. N. Holben (1997), Operational remote sensing of tropospheric aerosol over land from EOS moderate resolution imaging spectroradiometer, J. Geophys. Res., 102, 17051-17067.

Kaufman Y. J., Ilan Koren, Lorraine A. Remer, Daniel Rosenfeld and Yinon Rudich (2005), The Effect of Smoke, Dust and Pollution Aerosol on Shallow Cloud Development Over the Atlantic Ocean, PNAS - Proceedings of the National Academy of Sciences, Vol 102 (32), 11207-11212.

Keil, A., and J. M. Haywood (2003), Solar radiative forcing by biomass burning aerosol particles during SAFARI 2000: A case study based on measured aerosol and cloud properties, J. Geophys. Res., 108(D13), 8467, doi:10.1029/2002JD002315.

Loeb, N. G., Kato, S., Loukachine, K., and Manalo-Smith, N. (2005), Angular distribution models for top-of-atmosphere radiative flux estimation from the Clouds and Earth's Radiant Energy System instrument on the Terra satellite. Part 1 methodogy., J. Atmos. Ocean. Tech., 22, 338–351.

McGill, M. J., M. A. Vaughan, C. R. Trepte, W. D. Hart, D. L. Hlavka, D. M. Winker, and R. Kuehn (2007), Airborne validation of spatial properties measured by the CALIPSO lidar, J. Geophys. Res., 112, D20201, doi:10.1029/2007JD008768.

Myhre, G., T. K. Berntsen, J. M. Haywood, J. K. Sundet, B. N. Holben, M. Johnsrud, and F. Stordal (2003), Modeling the solar radiative impact of aerosols from biomass burning during the Southern African Regional Science Initiative (SAFARI-2000) experiment, J. Geophys. Res., 108(D13), 8501, doi:10.1029/2002JD002313.

Rajeevan and Srinivasan (2000), Net cloud radiative forcing at the top of the atmosphere in the Asian monsoon region, *Journal of Climate* 13 (2000), 650–657.

Redelsperger, J.L., et al. (2006), African monsoon multidisciplinary analysis (AMMA): An international research project and field campaign, Bull. Am. Meteorol. Soc., 87, 1739–1746.

Rosenfeld, D., et al. (2001), Desert dust suppressing precipitation: A possible desertification feedback loop, Proc. Natl. Acad. Sci. U. S. A., 98(11), 5975– 5980.

Ross, K. E., S. J. Piketh, R. T. Bruintjes, R. P. Burger, R. J. Swap, and H. J. Annegarn (2003), Spatial and seasonal variations in CCN distribution and the aerosol-CCN relationship over southern Africa, J. Geophys. Res., 108(D13), 8481, doi:10.1029/2002JD002384.

Solomon, S., D. Qin, M. Manning, Z. Chen, M. Marquis, K.B. Averyt, M. Tignor and H.L. Miller (2007), Climate Change 2007: The Physical Science Basis. Contribution of Working Group I to the Fourth Assessment Report of the Intergovernmental Panel on Climate Change (IPCC), Cambridge University Press, Cambridge, United Kingdom and New York, NY, USA.

Su, J., Jianping Huang, Qiang Fu, P. Minnis, Jinming Ge and Jianrong Bi (2008), Estimation of Asian dust aerosol effect on cloud radiation using Fu-Liou radiative model and CERES measurements, Atmos. Chem. Phys., 8, 2763–2771, www.atmos-phys.net/8/2763/2008/.

Swap, R.J. et al. (2002), The Southern Africa Regional Science Initiative (SAFARI 2000): Overview of the dry season field campaign, S. Afr. J. Science., 98, 125-130.

Twohy, C. H., et al. (2009), Saharan dust particles nucleate droplets in eastern Atlantic clouds, Geophys. Res. Lett., 36, L01807, doi:10.1029/2008GL035846.

Twomey, S. (1977), The influence of pollution on the shortwave albedo of clouds, J. Atmos. Sci., 34, 1149–1152.

Weare, B. C. (1997), Climatic variability of cloud radiative forcing, Quart. J. Roy. Meteor. Soc., 123, 1055–1073.

Wielicki, B. A., et al. (1996), Clouds and the Earth's radiant energy system (CERES): An Earth observing system experiment, Bull. Am. Meteorol. Soc., 77, 853– 868.

Winker, D. M., J. R. Pelon, and M. P. McCormick (2003), The CALIPSO mission: Spaceborne

lidar for observation of aerosols and clouds, in Lidar Remote Sensing for Industry and Environment Monitoring III, edited by U. Singh, T. Itabe, and Z. Liu, Proc. SPIE Int. Soc. Opt. Eng., 4893, 1–11.

Winker, D. M., M. A. Vaughan, A. H. Omar, Y. Hu, K. A. Powell, Z. Liu, W. H. Hunt, and S. A. Young (2009), Overview of the CALIOP Algorithms, J. Atmos. Oceanic Technol., submitted.

Zardecki, A. and Deepak, A. (1983), Forward Multiple Scattering Corrections as a Function of the Detector Field of View, Appl. Opt., 22, 2970.

Table 1. Description of Profile Types

Profile Type	Constraints	Total Samples
Pristine	no cloud or aerosol layers present	722
Cirrus	aerosol-free profile with thin cirrus cloud	1447
High Convective Cloud (HCC)	aerosol-free profile with high convective cloud	2968
Low Cloud	aerosol-free profile with low cloud	4673
Dust	cloud-free profile with dust layer	2505
Smoke	cloud-free profile with smoke layer	8476
Dust-Low Cloud (DLC)	profile with a low cloud and dust layer	2430
Smoke-Low Cloud (SLC)	profile with a low cloud and smoke layer	1140
Dust-Cirrus Cloud (DC)	profile with a thin cirrus cloud and dust layer	304
Smoke-Cirrus Cloud (SC)	profile with a thin cirrus cloud and smoke layer	244

Table 2. Three Year Mean of Aerosol Properties

Aerosol Type	Optical Depth	Depol Ratio	Lidar Ratio	Height (km)
Smoke	0.27	0.04	50.57	0.94
Dust	0.24	0.19	39.85	2.84

Table 3. Three Year Mean of Cloud Microphysical Properties

Profile Type	Optical Depth	CIAB (sr-1)	Height (km)
SC	0.39	0.0114	12.34
DC	0.37	0.0112	12.29
Cirrus	0.53	0.0152	11.75
SLC	NA	0.0374	1.40
DLC	NA	0.0324	1.29
Low Cloud	NA	0.0570	1.93

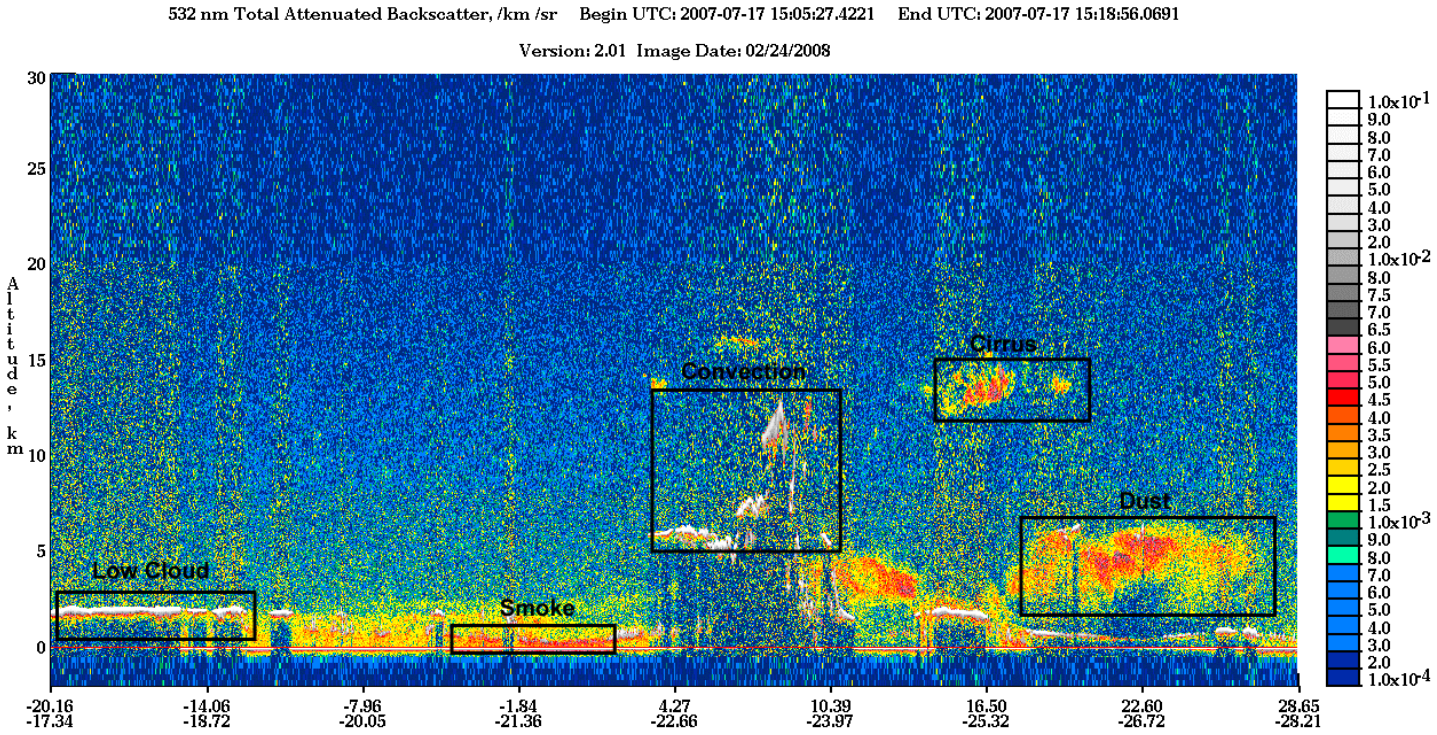

Figure 1. The 532 nm total attenuated backscatter (km^{-1}/sr^{-1}) image from the CALIOP lidar for the daytime CALIPSO track over the Tropical Atlantic on 17 July 2007. The black boxes identify the cloud and aerosol layers which serve as the basis of the ten profile types used in this study (http://www-calipso.larc.nasa.gov/products/lidar/browse_images/show_calendar.php).

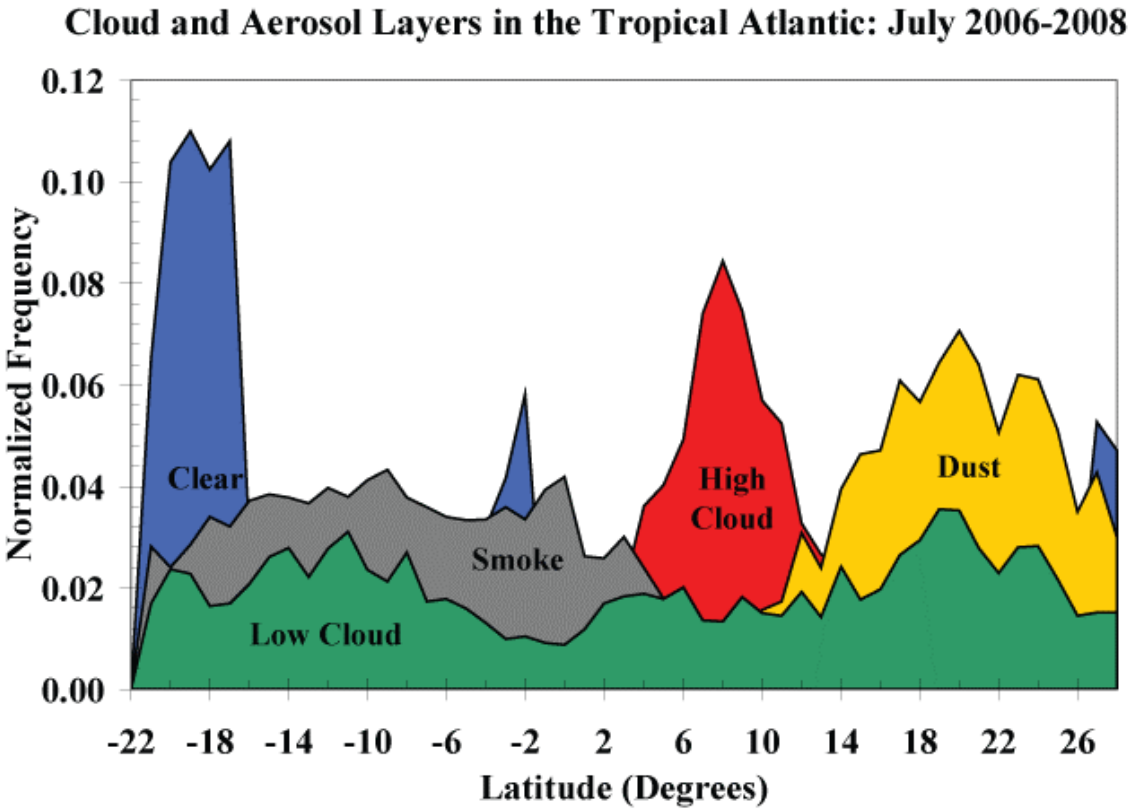

Figure 2. The frequency of the latitudinal occurrence of high cloud (red), low cloud (green), dust (yellow), smoke (grey), and clear (blue) profiles for all 3 years of July data, normalized to the total number of that phenomena's observations over all latitudes.

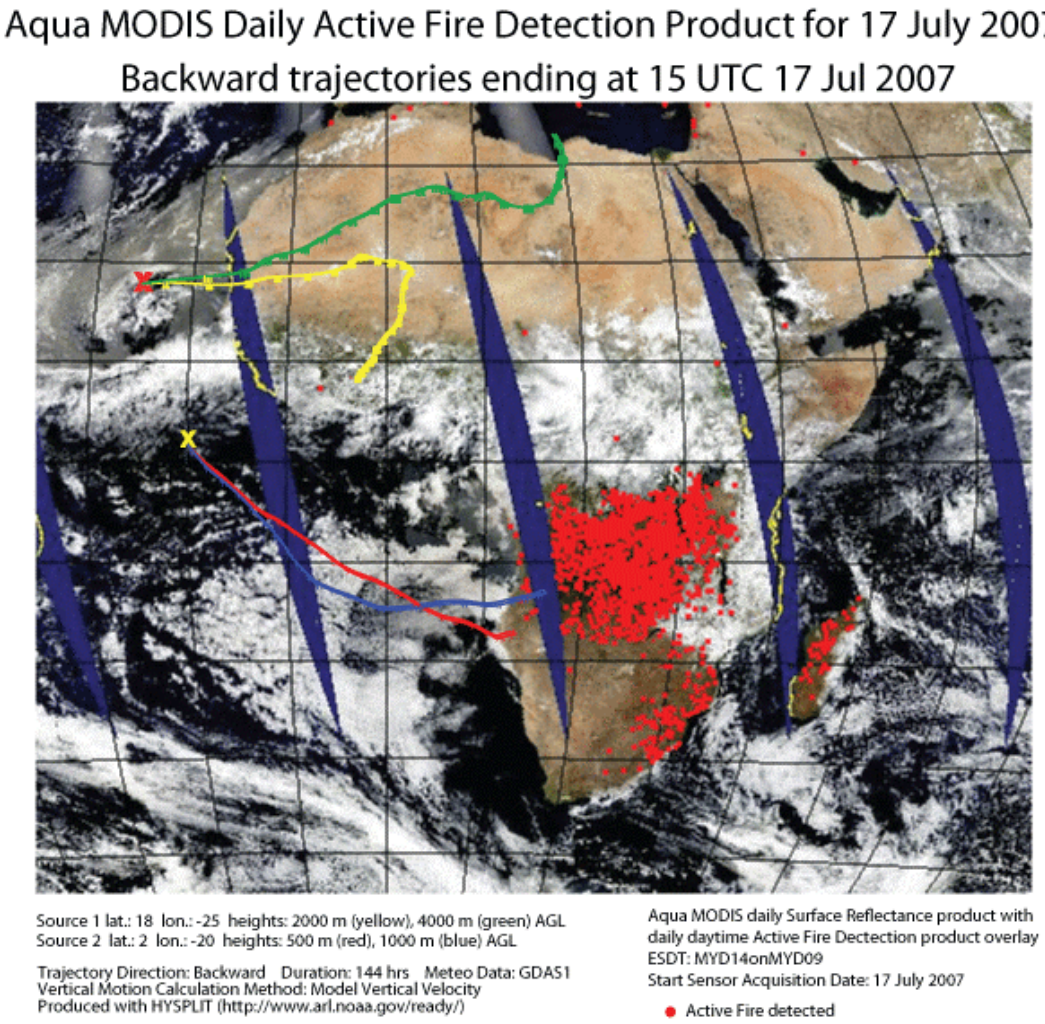

Figure 3. Back trajectories from NOAA HYSLPIT (http://www.arl.noaa.gov/ready/hysplit4.html) and GDAS Meteorological fields initialized at 18 N, 25 W and 2 S, 20 W for 17 July 2007 at 1500 UTC are overlaid on MODIS daily active fire detection product for 17 July 2007 (http://landweb.nascom.nasa.gov/cgi-bin/browse/browse.cgi). The active fires are indicated by the red dots.

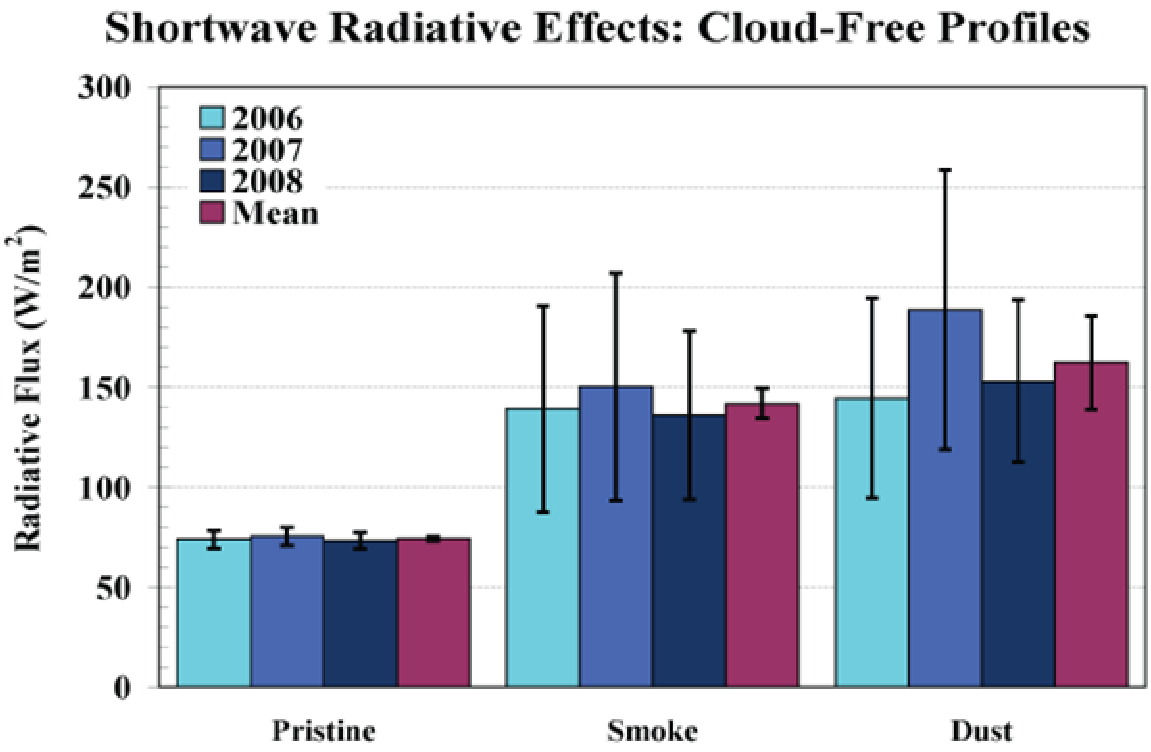

Figure 4. The 2006, 2007, 2008 and 3-year mean instantaneous SW TOA radiative fluxes (W/m^2) for all cloud-free profiles (Pristine, Smoke, Dust). The black error bars represent +/- one standard deviation.

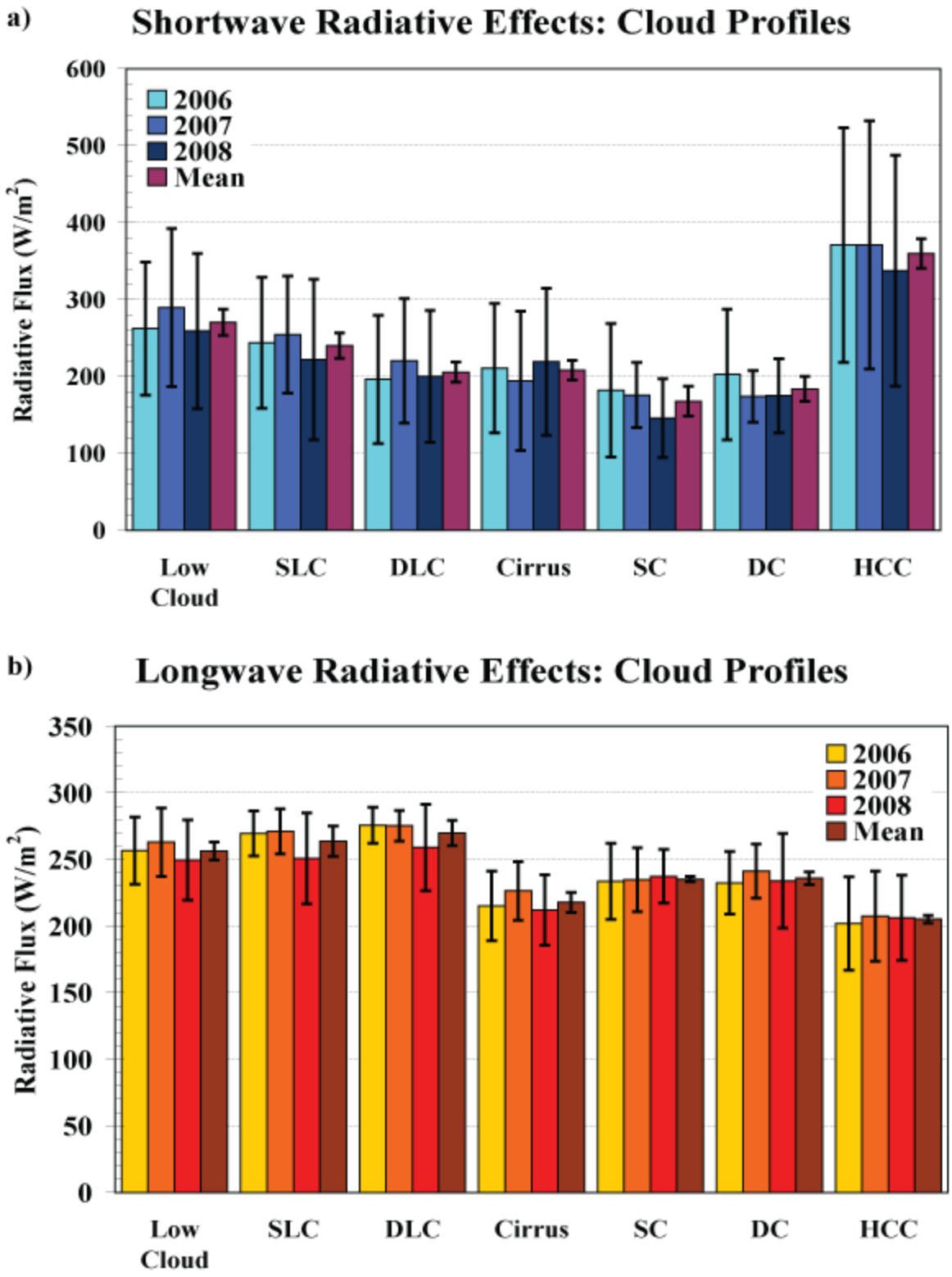

Figure 5. The instantaneous SW (a) and LW (b) TOA radiative fluxes (W/m^2) for all cloud profiles for 2006, 2007, 2008 and 3-year mean. The black error bars represent +/- one standard deviation. Refer to Table 1 for the profile type abbreviations.

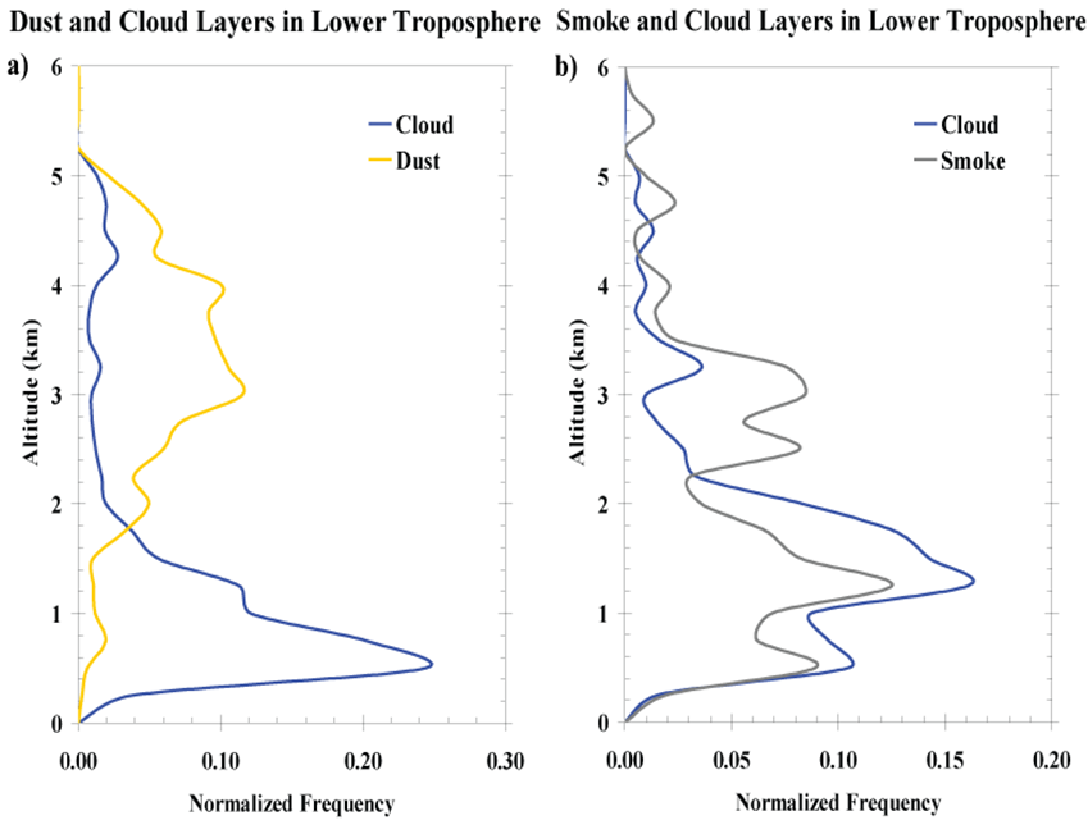

Figure 6. The frequency of the altitude (km) of (a) low cloud and dust layers from DLC profiles and (b) low cloud and smoke layers from SLC profiles for all 3 years of July data. The frequency is normalized using the total number of DLC and SLC profiles shown in Table 1.

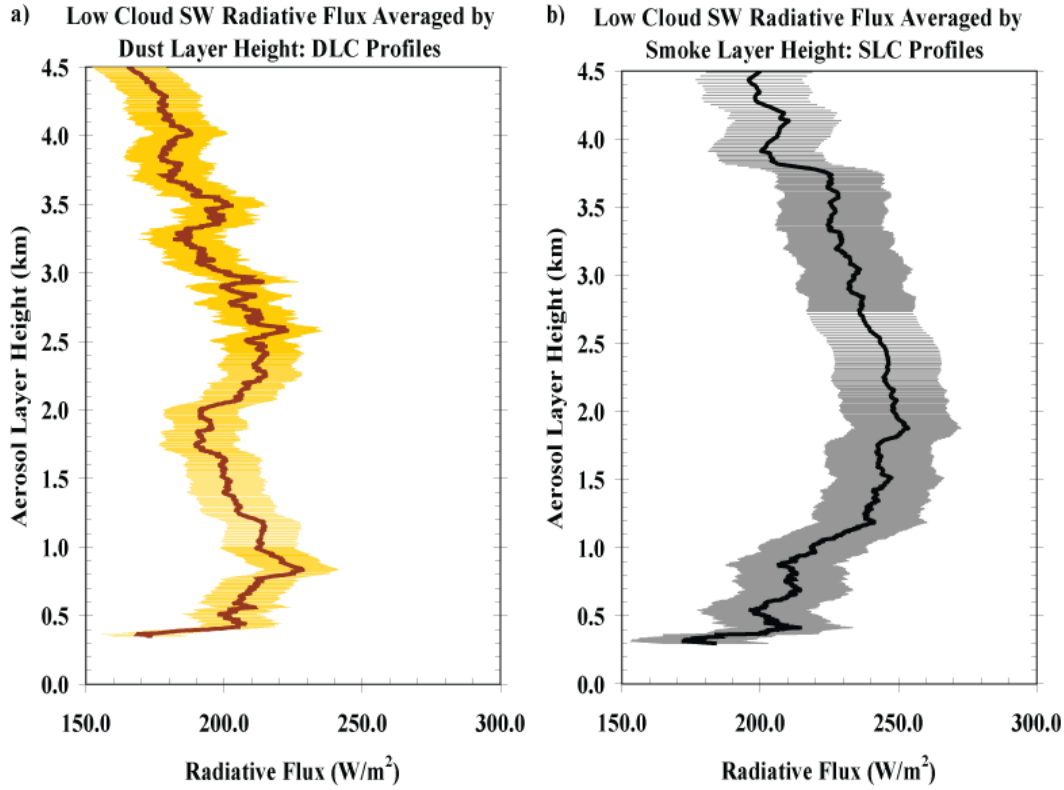

Figure 7. The running average of instantaneous SW TOA radiative fluxes (W/m^2) as a function of aerosol layer height from the (a) DLC profiles and (b) SLC profiles for all 3 years of July data. The gold (a) and grey (b) shaded area represent +/- one standard deviation.